SPALLATION NEUTRON SOURCE RADIATION SHIELDING ISSUES

R. T. Santoro, Y. Y. Azmy, J. M. Barnes, J. D. Drischler,
J. O. Johnson, R. A. Lillie, G. S. McNeilly
Oak Ridge National Laboratory
P. O. Box 2008, MS 6363
Oak Ridge, TN 37832-6363
423-574-6084

ABSTRACT

This paper summarizes results of Spallation Neutron Source calculations to estimate radiation hazards and shielding requirements for activated Mercury, target components, target cooling water, and ^{7}Be plateout. Dose rates in the accelerator tunnel from activation of magnets and concrete were investigated. The impact of gaps and other streaming paths on the radiation environment inside the test cell during operation and after shutdown were also assessed.

I. INTRODUCTION

The purpose of a spallation neutron source is to produce neutrons for research and commercial applications. Energetic charged particles and neutrons resulting from 1 GeV proton reactions in the Spallation Neutron Source (SNS) Mercury (Hg) target will challenge designers to provide adequate shielding for personnel and equipment during both operation and after shutdown. Levels of activation throughout the SNS accelerator target system and test cell will be high. SNS radiation protection policy has established 0.25 mrem/h as the dose rate limit for accelerator operation and maintenance personnel. Higher dose rates may be allowed during emergencies or accidents.

This paper summarizes some typical shielding issues facing design engineers. Results of calculations to determine the radiation environment inside the accelerator tunnel, target region, test cell, and other critical locations during and after shutdown are presented. Also discussed are problems arising from gaps and other penetrations in primary shielding and the impact on personnel dose rates of activated Hg, target cooling water, and ^{7}Be plateout.

When shielding problems are identified, preliminary calculations based on relatively simple models combined with one-dimensional radiation transport methods are often sufficient to establish bounds that edify the magnitude of the radiation and concomitant shielding requirements. These calculations also serve to provide input data to multidimensional Monte Carlo and discrete ordinates calculations of complex SNS systems and essential information for project engineers.

II. SHIELDING ISSUES

Interactions of 1 GeV protons in the SNS Hg target generate large quantities of energetic neutrons (>20 n/p). Neutrons emitted in the same direction as the beam, i.e. 0º, will have energies nearly as high as the incident protons. Although the neutron energy decreases with increasing angle, the spallation neutron spectrum is mostly forward peaked. Neutrons produced in spallation reactions will also generate “secondary” neutrons via (n,xn) reactions as they migrate through the primary and secondary shielding. Neutrons in the system will range from ~1 GeV to thermal energy.

The radiation shielding required for the SNS differs from fission reactors and some high-energy charged particle accelerators. Shield designers are faced with the dilemma of minimizing the damaging effects of these neutrons on personnel and equipment while striving to minimize the overall shield costs. Depending on its location, radiation shielding must provide protection against the (1) primary neutrons born in the spallation reactions, (2) secondary neutrons and gamma-rays from (n,xn) and (n,γ) reactions, respectively, and (3) gamma-rays from neutron activated materials. Additional discussions of SNS radiation shielding problems may be found in the papers by Johnson, et. al.(1), Odano, et. al.(2) and Gabriel, et. al.(3).

III. ASSESSMENT OF SPECIAL SHIELDING PROBLEMS

Typical SNS shielding/radiation problems are illustrated. The examples do not cover all of the shielding questions that exist or may arise as the design progresses. Illustrations are given for problems associated with the linac tunnel, target shielding, activated water, Hg, ^{7}Be plateout and gaps and penetrations in primary shielding. Results of one-dimensional discrete-ordinates radiation transport methods that yield rapid solutions to provide design guidance to engineers are reported.

III.a Dose Rate Inside the SNS Linac Tunnel from Activation of the Magnet Copper Conductor and the Concrete Walls

Personnel access inside the SNS linac tunnel for maintenance and other operations will be determined by the activation of the beam focusing and steering magnets and the concrete tunnel walls. Losses that occur during transit of the proton beam through the linac will result in reactions in the beam focusing magnets. Primary charged particles and secondary neutrons produced in these reactions will activate the magnet while secondary neutrons escaping from the magnet will activate the surrounding concrete walls.

The activation of a magnet copper conductor and the concrete in the linac tunnel walls due to proton beam losses was estimated for proton beam energies of 333, 667 and 1000 MeV. Line losses were assumed to be 1 nA/m for all proton energies. For the purpose of this work, the proton beam was taken to be incident on a 1-m-long copper cylinder (radius = 0.075m) placed in the center of a 30-m-long concrete lined tunnel. This geometry yields an overestimate of the radionuclide production in the magnet and the neutron leakage into the surrounding concrete, so the results are conservative.

The interior dimensions of the tunnel are 4.6x4.6 m^2 with a concrete wall thickness of 0.46 m and surrounded by 9 m of soil. The production of radionuclides in the copper and concrete were calculated previously (1,2) using the High Energy Transport Code, HETC (4) in combination with the MCNP (5) code to transport low energy (≤20 MeV) neutrons. The radionuclide production was used in the ORIHET (4) code to generate the decay gamma-ray spectra (2). Photon spectra from activation of the copper and concrete walls were calculated as a function of the incident proton-beam energy. Exposure time was taken to be 30 years corresponding to the total operating lifetime of the SNS. The spectra at four hours after accelerator shutdown were used as the source terms to estimate the dose rate inside the accelerator tunnel as a function of incident proton energy. Calculations were performed using the one-dimensional transport code ANISN (6) with a cylindrical geometry model of the copper and tunnel walls.

Fig. 1 shows the total dose rate (copper plus concrete) inside the tunnel as a function of distance from the tunnel centerline and as a function of incident proton energy. The dose rate is dominated by the activation of the copper and it increases with increasing proton energy. At 57.5 cm from the centerline (50 cm from the edge of the copper cylinder), the dose rates due to the activated copper are 15, 45, and 65 mrem/h, respectively, for incident proton energies of 333, 667, and 1000 MeV. At distances ≥1 m, the dose rates drop by more than a factor of two. The contribution to the dose rate in the tunnel from the activated concrete is less than two percent of the copper dose rate at all energies.

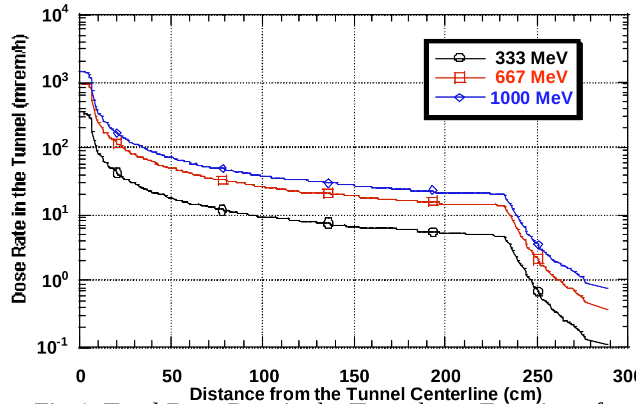

Fig.1. Total Dose Rate in the Tunnel as a Function of Distance from the Tunnel Centerline and Incident Proton Energy (30 Years Irradiation 4 Hours After Shutdown)

Some analysts prefer to report these data following 100 days of operation. The activation dose rates after 100 days of irradiation are lower, on the average, by about 25%. The dose rates at 50-cm beyond the copper are 11, 30 and 48 mrem/h, respectively, for beam energies of 333, 667 and 1000 MeV. At distances of ≥1 m, the corresponding dose rates are ~7, ~12, and ~25 mrem/h.

III.b Shielding Options for the Hg Target

Proper shielding of the target monolith is a critical issue facing SNS designers. As originally envisioned, this shield was to be constructed mainly of steel except for regions closest to the Hg target that are 0.8 m of 80% Pb-20% H_2O followed by 0.7 m of 80% Carbon Steel (Fe+5%C)-20% H_2O. The high cost of both material and fabrication for this configuration prompted designers to seek a less costly option having equivalent shielding performance. The availability of large quantities of lead prompted replacement of the steel with lead.

One-dimensional radiation transport calculations were performed to determine optimum configurations with both lead and lead mixtures replacing the steel. A fourteen-region, one-dimensional model of the monolith and surrounding concrete biological shield summarized in Table 1 was used in the analysis.

In the original configuration, the regions labeled "XXX" were comprised of carbon steel (CS). The merits of replacing these with Pb and lead mixtures were assessed. In the CS configuration, the total (n+γ) contact dose rate at the outside surface of the concrete biological shield was calculated to be 5.3 µrem/h. (At 1 mA proton beam current.) Replacing CS in regions 6, 9, and 12 with pure Pb and maintaining the same compositions elsewhere, increased the dose rate to 0.11 mrem/h. The increase is due to higher production of secondary gamma rays from low energy neutron reactions in lead and poor attenuation of the low-energy neutrons (En ≤ 20 MeV).

Table 1. One-Dimensional Model of
the Target Monolith and Biological Shield

Region	T (m)	Material
1	0.20	Void
2	0.80	80% Pb-20%H_2O
3	0.75	80%SS-20%H_2O
4	0.05	SS
5	0.025	SS
6	1.05	XXX
7	0.025	SS
8	0.025	SS
9	1.05	XXX
10	0.025	SS
11	0.025	SS
12	1.05	XXX
13	0.025	SS
14	1.00	Concrete

Several materials were proposed to replace the CS in regions "XXX". These included Borated Pb (0.5% ^{10}B), Cadmium Loaded Pb (0.5% Cd) and combinations of Cement (Borated and Nonborated) and Pb shot. The Borated and Cadmium-loaded Pb options, though neutronically advantageous, are impractical because of the difficulty to obtain homogeneous mixtures. Replacing the SS structure (regions 4, 5, 7, 8, 10, 11, and 13) with Borated SS was also evaluated.

The recommended configuration in terms of cost and fabrication consists of pure Pb in regions 6 and 9, a Borated Cement-Pb shot (65%Pb) in region 12 and Borated Concrete in the biological shield. The contact dose rate outside the biological shield was calculated to be 2.3 μrem/h. When voids, gaps, and manufacturing tolerances are taken into account, the contact dose rate increases by a factor of ~3 but is still well below the allowed dose rate.

Shields using other combinations of materials listed in Table 1 were also shown to be neutronically effective but were either difficult to fabricate or impossible to make with uniform consistency.

III.c Contact Dose Rates from ^{16}N Decay in the SNS Target Cooling Water Loop, Be-D_2O Inner Plug and Ni Outer Plug

Water flowing through the SNS target cooling water loop, Be-D_2O Inner Plug and Ni Outer Plug is activated via ^{16}O (n,p) ^{16}N reactions (E_{th} = 10 MeV). ^{16}N decays with a 7.13 second half-life with the emission of two energetic gamma rays: E_γ = 6.17 MeV (69%) and E_γ = 7.12 MeV (4.8%).

Calculations to estimate the contact dose rate from activated water exiting the coolant loop and inner plug immediately after the SNS shutdown following operation at 1 MW of beam power were performed. Water flow rates and hold up times were not taken into account nor was the self-shielding of the water or the shielding of the water pipe walls.

Activation levels of the water exiting the target cooling water loop, Be-D_2O inner plug and Ni outer plug at shutdown are 3.59 TBq (97 Ci), 4.85 TBq (131 Ci) and 1.77 TBq (47.9 Ci), respectively.

The dose rate at 1 cm from the water can be obtained using

$$D_r = \sum (Bq(E\gamma)/4\pi)^* f_E *FTD$$

where Bq(Eγ) is the disintegration rate (photons/s) of the activated water, f_E is the fraction of the time the activated water decays with the emission of a photon having energy Eγ (MeV), and FTD is the flux to dose conversion factor (rad $h^{-1}/\gamma\ cm^{-2}\ s^{-1}$). The factor of 4π converts Bq(Eγ) from photons/s to $\gamma\ cm^{-2}\ s^{-1}$. The sum is taken over the number of photons with energy Eγ emitted from the activated products.

The dose rates at 1 cm from the water are summarized in Table 2. The dose rate calculated here is due only to the decay of ^{16}N. Contributions from the decay of ^{17}N, ^{19}O and other radioisotopes produced in water are not included.

Table 2. Calculated Dose Rates in the Cooling Water Loops

Photon Flux	f_E (%)	FTD	Dose Rate (Mrad h^{-1})
Cooling Water Loop			
2.86 x 10^{11}	68 at 6.17 MeV	6.25 x 10^{-6}	1.21
2.86 x 10^{11}	4.8 at 7.12 MeV	6.90 x 10^{-6}	0.09
		Total	1.30
Be-D_2O Inner Plug			
3.64 x 10^{11}	68 at 6.17 MeV	6.25 x 10^{-6}	1.55
3.64 x 10^{11}	4.8 at 7.12 MeV	6.90 x 10^{-6}	0.12
		Total	1.67
Nickel Outer Plug			
1.41 x 10^{11}	68 at 6.17 MeV	6.25 x 10^{-6}	0.60
1.41 x 10^{11}	4.8 at 7.12 MeV	6.90 x 10^{-6}	0.05
		Total	0.65

III.d Shielding of Activated Mercury: Bulk Quantities and in Pipes

The mercury flowing through the SNS target will become highly activated and decay by the emission of energetic gamma rays. The photon decay spectrum for Hg at 60 seconds after SNS shutdown following one year of operation is shown in Fig.2.

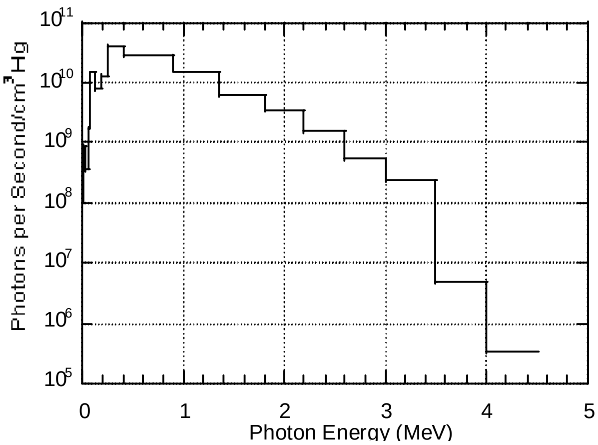

Fig. 2. Hg Decay Photon Spectrum at Shutdown (Photons / second vs. Photon Energy)

The mercury flows continuously into and out of the target assembly through stainless steel pipes. These pipes pass close to radiation sensitive sensors and other instrumentation that can be damaged by the high flux of unattenuated decay gamma rays from the Hg. In addition, the Hg may be held up in tanks that are also adjacent to radiation sensitive equipment.

One dimensional transport calculations were performed to determine the dose rate as a function of iron shield thickness surrounding 4- and 8-cm-radius Hg filled spheres and 4- and 8-cm-radius Hg filled pipes. The sphere and pipe dimensions are arbitrary but are expected to be similar to the Hg flow pipes and small hold-up tanks in the SNS.

The results are shown in Fig. 3. Plotted in the figure is the dose rate as a function of the thickness of iron surrounding the spheres and pipes. For the pipe configuration, the dose rate is in units of mrem/h/(cm of pipe length). The flat portions of the curves between 0 - 4 cm and 0 - 8 cm shows there is essentially no self shielding of the decay photons by the Hg. The contact dose rate increases with increased Hg volume as expected.

III.e Dose Rate Outside the SNS Target Maintenance Hot Cell From Radiation Streaming through the Clearance Gaps Surrounding the Target Carriage

Insertion and withdrawal of the SNS target carriage into and out of the target monolith requires clearance gaps between the carriage surfaces and the monolith walls, ceiling and floor to facilitate movement of the carriage. During accelerator operation, neutrons produced in the Hg target and surrounding materials will migrate through the moderator-reflector and shielding surrounding the target. The transmitted neutrons and secondary gamma rays will impinge on the front face of the carriage. The shielding provided by the carriage itself reduces the radiation leaking into the posterior target-maintenance cell. The dose rate outside the cell walls is less than 0.25 mrem/h. SNS designers are concerned about the impact of radiation streaming through these gaps on the dose rate outside the maintenance cell.

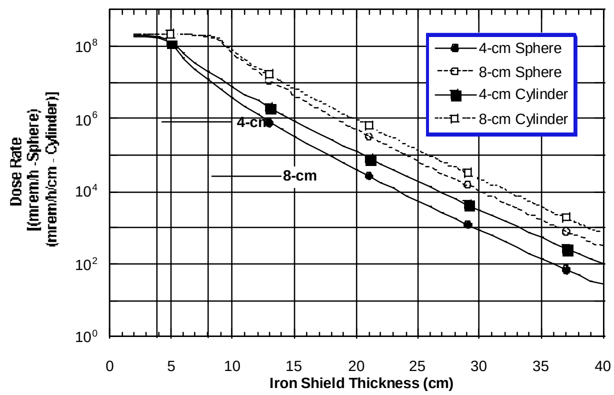

Fig. 3. Dose Rate vs. Iron Shield Thickness

Gap Geometry: It was assumed that the target carriage is a solid assembly surrounded on all sides by a 7-mm-wide gap. The carriage cross section is 1.72m x 1.72 m over the entire 5-m length of the assembly.

Neutron Source: Neutrons produced from the reactions of 1-GeV protons in the Hg target were calculated previously by R. A. Lillie and J. M. Barnes (7), using the High Energy Transport Code, HETC. Neutron emission in the angular intervals between 0° and 20° was used as the source term for this analysis.

Neutron and Photon Spectra Incident on the Face of the Carriage: Neutrons produced in the Hg target migrate through a Pb-D_2O reflector and iron shield assembly. The neutron and gamma rays that leak out of the iron are incident on the face of the target carriage and the gaps.

The leakage from the moderator-reflector-shield assembly was calculated using the one-dimensional radiation transport code ANISN with cross-sections taken from the HILO library (8). These data were obtained using a spherical geometry approximation of the assembly and the material compositions summarized in Table 3. Scattering was approximated using a P_5 Legendre polynomial expansion of the cross sections with an S_{64} angular quadrature to estimate the angular flux. Calculations were carried out to estimate the angular distribution of neutrons and gamma rays at the outer surface of the iron shield.

Table 3. One Dimensional Model of the SNS Target Moderator and Reflector
(T = Thickness)

T (Δr) (cm)	T (Σr) (cm)	Material	Atomic Composition (atom/cm^3 x 10^{-24})
1	1	Neutron Source Region	0
19	20	Void	0
100	120	Lead Moderator	Pb: 0.0297
50	170	Steel Reflector	Fe: 0.0840, Mn: 0.000388, C: 0.000782, Si: 000421

Only the neutrons and gamma rays that leak out of the iron shield in the forward direction will have a chance of entering gaps. The forward emitted component of the angular flux, ϕ_F [(n cm^{-2} s^{-1} sr^{-1})/(proton s^{-1}) in the interval between 0 and 3° calculated using the leakage source was taken as the source incident on the mouth of the gap.

The incident spectrum was also scaled using energy dependent factors derived from a previous three-dimensional streaming calculation by L. Charlton (9). The neutron flux derived here was increased by factors of five to 2000 depending on energy and the gamma-ray flux was increased by a factor of 1000.

Flux Exiting the Gap: The flux at the rear of the gap, ϕ_R, (n cm^{-2} s^{-1}) due to streaming can be estimated using the following relation.

$$\Phi_R = \phi_F\, \Omega_{gap}.$$

Ω_{gap} is the solid angle subtended by the gap. For a rectangular duct the solid angle is given by

$$\Omega_{gap} = \tan^{-1}[ab/4zD]$$

$$D = [z^2 + (a/2)^2 + (b/2)^2]^{1/2}$$

where a and b are the width and breadth of the gap and z is the length. As noted above, all gaps were assumed to be the same, i.e., a = 7, b= 1720 and z = 5000 mm. Then, $\Omega_{gap} = 1.2 \times 10^{-4}$ sr.

The flux at the rear of the gaps, Φ_R, was used to calculate the dose rate outside the maintenance-cell concrete wall.

Calculation of the Dose Rate Outside the Heavy Concrete Maintenance Cell: The dose rate outside the heavy-concrete maintenance cell wall was calculated using ANISN with a spherical geometry model to approximate the shielding around the maintenance cell. The neutron and gamma ray source term (p s^{-1}) was calculated using

$$S_n = 2(10\Phi_R)(4A_{gap})\, P_s\, f_s$$

where Φ_R has been multiplied by 10 to allow for the scattered flux exiting the gap, A_{gap} is the area of a gap (0.7 cm x 172 cm) multiplied by 4 to account for all gaps, P_s is the accelerator proton source strength, and f_s is a factor that is required to normalize the source to 4π steradians.

The uncollided flux exiting the gaps is essentially forward peaked. The lateral width of the gap will result, however, in uncollided neutrons exiting the gap at wide angles. The maximum angle is given by

$$\theta = \tan^{-1}(W_g/L_{tc}) = \tan^{-1}(172/500) = \sim 19°.$$

where W_g is the width of the gap and L_{tc} is the length of the target carriage.

These neutrons are incident on the surrounding concrete wall at "grazing" angles ≤θ. The maximum "straightahead" thickness of concrete the neutrons traverse before exiting the 100-cm–thick concrete maintenance wall, T_c, is

$$T = T_c/\sin(\theta) = 100/\sin(19°) = \sim 300 \text{ cm}.$$

Neutrons that are scattered while traversing the gap emerge at larger angles but these will be of lower energy and will be more rapidly attenuated in the concrete.

The dose rate behind 300-cm of concrete is given in Table 4.

Table 4. Dose Rate Outside the Concrete Maintenance Wall

Neutron Source (Solid Angle)	Neutron Source Strength, $P_s f_s$ (n/s)	Dose Rate Behind 300 cm of Heavy Concrete (µSv/h)
0 – 20 deg	7.4 x 10^{15}	0.53

The approximations made for this analysis lead to a conservative estimate of the dose rate outside the maintenance cell. The assumption that the radiation entering the gap corresponds to the forward directed (0 to 3°) component of the angular flux is an overestimate. This corresponds to the most intense component of the high-energy angular flux. The flux decreases a factor of ten or more for a small increase in angle. The angular distribution of the low energy neutrons is nearly constant with angle and, though the intensity is greater than the forward peaked component, the contribution to the dose rate outside the maintenance cell is small.

Modeling the radiation incident on the gaps in this way overestimates the dose rate outside the maintenance cell by at least an order of magnitude.

The assumption that the width of all gaps is the same increases the streaming flux by ~30%. Since the carriage is also narrower than it is tall, the angle at which the neutrons strike the sidewalls of the cell is smaller so the forward directed flux traverses a greater thickness of concrete.

In the actual carriage configuration, there are offsets in the gaps along the top and sides of the assembly. Ignoring offsets further reduces the high energy neutron streaming. An additional factor of 2 to 5 reduction in the dose rate is probable.

The dose rate reported in Table 4 is less than the recommended dose rate level of 0.25 mrm /h. Including the conservatism implied above, the impact of streaming through the clearance gaps on the dose rate outside the maintenance cell is tolerable.

III.f Radiation Streaming through the Mercury Loop in the SNS Target Carriage

Mercury is supplied to the SNS target through a pipe assembly that passes through the target carriage. The pipe assembly, shown in Fig. 4, referred to as the mercury loop is configured as a three-legged duct to reduce the radiation leaking through the pipe during a loss-of-mercury accident.

In a loss-of-mercury accident, 1 GeV protons can stream through the loop and react in the pipe and the carriage materials at the first bend producing charged particles and secondary neutrons. These particles, particularly the neutrons, can migrate through the pipe and leak from the rear of the carriage into the target maintenance cell.

For this work, it was assumed that the mercury loop consists of a 6.25-cm-radius pipe imbedded in a 4.85-m-long solid steel block. For the case when the pipe is filled with mercury, it is assumed that the radiation attenuation provided by the block and the filled pipe meets SNS shielding criteria. The two straight sections of the pipe are 202 and 212 cm long, respectively. The length of the pipe through the second 45° bend is ~30 cm. The straight sections of the pipe are separated by ~3 pipe radii.

A series of Monte Carlo calculations using the High Energy Transport Code, HETC, to estimate neutron streaming through a two-legged pipe (one bend) configuration were carried out previously (7). The results, plotted in Fig.5, show that a 450-cm-long duct following the initial bend reduces the incident radiation by five orders of magnitude.

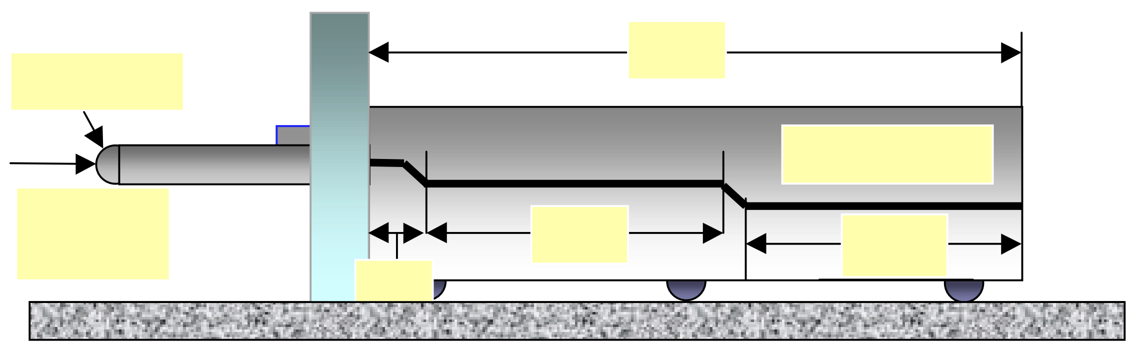

Fig. 4. Schematic Diagram of the Target Carriage and Mercury Loop

These data can be used to roughly estimate the attenuation through the three-legged duct (two bends; see Fig. 4, by superimposing the curve between 50 and 202 cm in Fig. 5 onto the point at 202 cm to account for the third leg in the pipe. The result is shown in Fig.6. Introducing the second bend in the pipe attenuates the radiation by about seven orders of magnitude.

A Monte Carlo calculation was also performed to estimate the neutron population and energy spectra as a function of distance along the duct axis. In this analysis, the target carriage-mercury loop was modeled in detail. A line beam of 1-GeV protons was taken to be incident on the mouth of the pipe. Neutrons produced from proton reactions in the iron were tallied as a function of location in the duct.

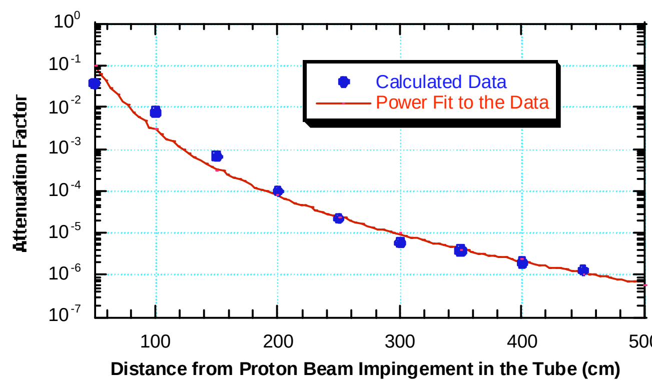

Fig. 5. Attenuation as a Function of Pipe Length

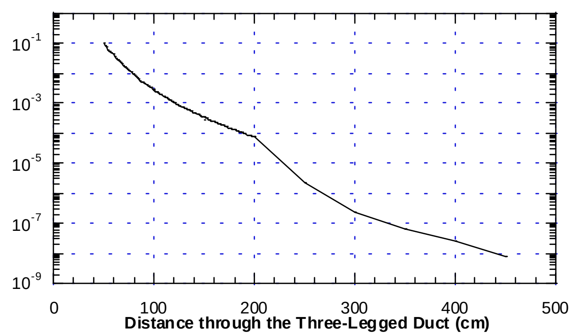

Fig. 6. Estimated Attenuation in the Three-Legged Duct

Tally surfaces were positioned along the duct axis to score neutrons passing through the iron structure and the open duct. The cross-sectional area of the duct opening is <1% of the cross-sectional area of the carriage. One million source particles and their progeny were transported to achieve good statistical sampling particularly through the front elements of the duct. The neutron population, energy, and angular distribution were tallied. The energy was recorded in eight energy bins between 0 and 700 MeV while their angular distributions were scored in two broad bins between $-1<\mu<0$ and $0<\mu<1$.

The attenuation of the neutron current for all energies inside the duct with $0<\mu<1$ is shown in Fig. 7. The curve is an exponential fit to the calculated data. The attenuation is approximately seven orders of magnitude. The error bars reflect the standard deviation of the neutron population. The large attenuation of the bulk shielding material and the small opening of the duct lead to poor sampling of the neutron population at long distances through the loop.

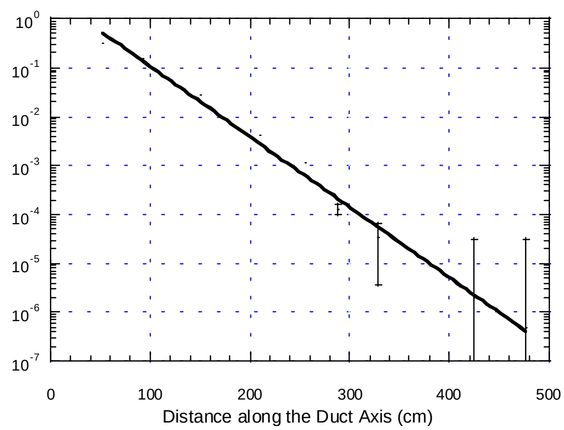

Fig. 7. Calculated Attenuation through the Three-Legged Duct

The energy distribution of the neutrons as a function of location in the duct is shown in Table 7. The point to note is the rapid decrease in energy with increased distance through the duct. Despite the poor statistics near the terminus of the duct, the trend in these data suggest that the energies of neutrons that do leak out of the duct are below 1 MeV.

Table 5. Energy Distribution of Neutrons inside the Duct as a Function of Location in the Duct

Dist	Neutrons/Source Proton $<E_n$							
(cm)	Energy Bin Boundaries (MeV)							
	10^{-5}	0.1	1	20	100	300	500	700
52.6	2.5-3	8.5-2	1.7-1	4.0-2	8.6-3	3.4-3	2.8-4	2.1-5
92.5	1.5-3	5.1-2	8.6-2	1.2-2	1.1-4	5.3-5	3.8-5	3.9-5
150	6.7-4	1.5-2	1.1-2	7.7-4	2.4-4	1.5-4	2.4-5	6.0-6
210	1.4-4	2.5-3	1.3-3	9.5-5	2.8-5	1.7-5	3.0-6	0.0
256	3.3-5	6.6-4	3.9-4	4.4-5	8.0-6	4.0-6	0.0	0.0
288	8.0-6	9.5-5	2.6-5	0.0	0.0	0.0	0.0	0.0
328	1.0-6	2.6-5	7.0-6	0.0	0.0	0.0	0.0	0.0
375	1.-6	1.-5	0.0	0.0	0.0	0.0	0.0	0.0
425	0.0	2.0-6	0.0	0.0	0.0	0.0	0.0	0.0
476	0.0	1.0-6	1.0-6	0.0	0.0	0.0	0.0.	0.0
Read 2.5-3 as 2.5×10^{-3}								

REFERENCES

1. J. O. Johnson, et. al., *Preliminary Shielding Assessment for the Proposed National Spallation Neutron Source (NSNS)*, Proceedings of the Topical Meeting on Nuclear Applications of Accelerator Technology, Albuquerque, NM, Nov. 16-20, 1997

2. N. Odano, J. O. Johnson, and R. A. Lillie, *Preliminary Shielding Analysis and Design of the Remote Maintenance Cells for the Proposed National Spallation Neutron Source (NSNS)*, Proceedings of the Topical Meeting on Nuclear Applications of Accelerator Technology, Albuquerque, NM, Nov. 16-20, 1997

3. T. A. Gabriel, et. al., *Target Station for the National Spallation Neutron Source*, Proceedings of the Topical Meeting on Nuclear Applications of Accelerator Technology, Albuquerque, NM, Nov. 16-20, 1997

4. T. A. Gabriel, et. al., *CALOR, A Monte Carlo Program Package for the Design and Analysis of Calorimeter Systems*, Oak Ridge National Laboratory, ORNL/TM-5619 (1977)

5. J. F. Briesmeister, Ed., *MCNP-A General Purpose Monte Carlo Code for Neutron and Photon Transport*, LASL Report LA-7396-M, Rev. 2 (Sept. 1986)

6. W. W. Engle, Jr., *A User's Manual for ANSIN: A One-Dimensional Discrete Ordinates Transport Code with Anisotropic Scattering*, Union Carbide Nuclear Division Report K-1693 (1967)

7. R. A. Lillie and J. M. Barnes, Oak Ridge National Laboratory, Private Communication (1999)

8. R. G. Alsmiller, Jr. and J. Barish, *HILO Neutron and Photon Multigroup Cross Sections for Neutron Energies <400 MeV*, Oak Ridge National Laboratory, ORNL/TM-7818 (June 1981)

9. L Charlton, Oak Ridge National Laboratory, Private Communication (1999)